

Sheets of branched poly(lactic acid) obtained by one-step reactive extrusion–calendering process: physical aging and fracture behavior

J. Cailloux · O. O. Santana · E. Franco-Urquiza ·
J. J. Bou · F. Carrasco · M. Ll. MasPOCH

Received: 4 November 2013 / Accepted: 1 February 2014 / Published online: 19 February 2014
© Springer Science+Business Media New York 2014

Abstract The architectural modifications of a linear poly(D,L-Lactide) acid (PD,L-LA) commercial grade were induced by a one-step reactive extrusion–calendering process using a styrene-glycidyl acrylate copolymer as reactive agent. The melt degradation was counteracted by chain extension and branching reactions, leading to a stabilization of the melt properties and an increase in the molecular weight. For such modified samples [poly(lactic acid) (PLA)-reactive extrusion (REX)], the rate of physical aging at 30 °C was investigated during 1 week in order to simulate industrial storage conditions. Fracture behavior of “de-aged” and “controlled aged” (1 week) samples was investigated using the essential work of fracture (EWF) methodology and the critical tip opening displacement at the crack propagation onset, respectively.

These analyses were complemented by digital image correlation analysis and inspection of the fractured surfaces by scanning electronic microscopy. As a result of the architectural modifications, the entanglement network density was increased. Those accounted for a slight decrease in the physical aging rate. Under uniaxial loading, aged reactive extrusion (REX) samples exhibited multiple crazing, leading to a slight increase in strain at break. Nevertheless, as a result of a similar dynamic environment of the entangled polymer coils, de-aged REX samples disclosed similar mechanical properties as compared to their neat counterparts. Regarding de-aged samples, the EWF analysis revealed no changes in the work required for the onset of crack propagation. However, the energy consumed up to the onset of crack propagation of aged PLA-REX samples decreased due to an apparently decreased network extensibility, promoting a premature craze–crack transition.

J. Cailloux · O. O. Santana (✉) · E. Franco-Urquiza ·
M. Ll. MasPOCH
Centre Català del Plàstic (CCP), Universitat Politècnica de
Catalunya (UPC), C/Colom, 114, 08222 Terrassa, Spain
e-mail: orlando.santana@upc.edu

J. Cailloux
e-mail: jonathan.cailloux@upc.edu

E. Franco-Urquiza
e-mail: edgar.adrian.franco@upc.edu

M. Ll. MasPOCH
e-mail: maria.lluisa.masPOCH@upc.edu

J. J. Bou
Department of Chemical Engineering, Universitat Politècnica de
Catalunya (UPC), Pavelló G, planta 1, Avenida Diagonal, 647,
08028 Barcelona, Spain
e-mail: Jordi.bou@upc.edu

F. Carrasco
Department of Chemical Engineering, Universitat de Girona
(UdG), Campus Montilivi s/n, 17071 Girona, Spain
e-mail: felix.carrasco@udg.edu

Keywords Poly(lactic acid) · Reactive extrusion ·
Physical aging · Enthalpy relaxation · Essential work of
fracture · Digital image correlation

Introduction

The constant increase in fossil fuel prices and the environmental impact of petrochemical plastics have encouraged researchers to find new solutions for the biodegradable plastics industry. Recent advances in manufacturing technologies allow for drastic decrease in production costs of poly(D,L-Lactide) acid (PD,L-LA) from renewable feed stocks. Nowadays, a better understanding of the properties led to an improved compatibility with various thermoplastics which in turn increased the commercial interest in PD,L-LA products [1, 2].

Due to the relatively fast cooling rates of industrial processes as compared to the crystallization rates of current commercial bioplastic grades, PD,L-LA items are generally found in their amorphous state [1]. As commercial PD,L-LA parts are usually employed in ambient conditions, they are used at a temperature below (but close) to T_g . Therefore, these thermodynamically unstable glasses tend toward an equilibrium state through slow segmental rearrangements over time. This phenomenon is commonly referred to as “physical aging” process and may have important drawbacks on the service life of polymer products and large-scale commercial applications. Based on temperature variable FTIR measurements, Pan et al. [3] reported a molecular conformational rearrangement during the aging process in which locally ordered domains are formed. Several previous works report a decrease in mechanical and fracture properties of aged material structures, promoting the ductile–brittle transition behavior [4, 5]. Although, aged PD,L-LA resins are characterized by their brittle behavior and low failure strain at room temperature, they are also classified as high-strength and high-modulus polymers. However, this brittleness does not only affect the end-use behavior but also the handling and processing, leading to important drawbacks in large-scale production [6, 7].

For a large number of amorphous polymeric systems, it is well established that the relaxation and deformation mechanisms are partially governed by the entanglement network density (ν_e) as well as by the intrinsic flexibility of their respective backbone [8, 9]. The latter may be related to the characteristic ratio C_∞ , characterizing the random coil nature of the polymer. Thus, high C_∞ values correspond to polymers that are loosely coiled (low flexibility of the backbone), while low C_∞ values correspond to tightly coiled polymers (high flexibility of the backbone). Several studies [8, 10] showed that the brittle behavior of amorphous poly(lactide) stereo-copolymers accounts for a low ν_e coupled with a high value of C_∞ . Regarding high-density polyethylene [11, 12], a larger ν_e may be a good solution to enhance the fracture performances of PD,L-LA resins. An increase in ν_e may be obtained through the insertion of long-chain branching which, according to Tangpasuthadol et al. [13] may also control the rate of enthalpy relaxation during the physical aging process. This enhancement may thereby extend the handling timeframe prior to a significant effect of the physical aging process. Several authors [14, 15] reported that reactive extrusion process is an attractive way in order to induce long-chain-branching topology in the poly(lactic acid) matrix, to stabilize the melt properties and to increase the molecular weight of the initial polymer.

In our previous study [16], structural modified PD,L-LA sheets were obtained through one-step reactive extrusion–

calendering process using a styrene-glycidyl acrylate copolymer as reactive agent. According to the rheological analysis performed on the resulting material [poly(lactic acid) (PLA)-reactive extrusion (REX)], it has been established that long-chain-branching topology was induced in the initially linear PD,L-LA matrix. Consequently, the melt strength as well as melt relaxation was increased through the creation of a higher entangled network density.

The current study focuses on the influences of such higher ν_e on the rate of enthalpy relaxation during 1 week in order to simulate industrial storage conditions. In addition, the dominant role of a change in the PD,L-LA entanglement network density on the fracture behavior of de-aged and physically aged samples has been investigated.

Experimental

Materials

A commercial PD,L-LA extrusion grade (Ingeo 4032D[®]), supplied by NatureWorks (Arendonk, Belgium) was used in this study. This grade contains about 2 % of D enantiomer molar content and a melt flow index of 6.4 ± 0.3 g/10 min (ASTM D1238-04c) [17]. A styrene-acrylic multi-functional-epoxide oligomeric agent (SAMfE) was employed as chain extender. It was kindly supplied by BASF (Ludwigshafen, Germany) (Joncryl-ADR-4300F[®]) in flake form with a T_g of 56 °C, a molecular weight of $5443 \text{ g}\cdot\text{mol}^{-1}$ and an epoxy equivalent weight of $433 \text{ g}\cdot\text{mol}^{-1}$ [16].

Sample preparation

Prior to extrusion, virgin PD,L-LA pellets were dried for 3 h at 80 °C in a PIOVAN hopper-dryer (DSN506HE, Venice, Italy) with a dew point of -40 °C and kept under the same conditions during the whole process. SAMfE was powdered using mortar and pestle and then stored overnight at room temperature under vacuum. Through one-step reactive extrusion–calendering process, the PD,L-LA grade was melt-blended with 0.5 wt% of SAMfE agent in a co-rotating twin-screw extruder 25 mm (L/D = 36) (KNETER 25X24D, COLLIN, Ebersberg, Germany) under a nitrogen blanket. The temperature profile was established from 150 °C in the feeding zone to 175 °C in the die with a screw speed of 40 rpm. In addition, vacuum was applied in the metering zone to remove volatiles created during the reactive stage. Finally, long-chain-branching PD,L-LA sheets with a nominal thickness of 1 mm and a nominal width of 100 mm were calendered (Techline CR72T, COLLIN, Ebersberg, Germany). The chill roll (D = 72 mm) temperature was set to 50 °C with a rotation

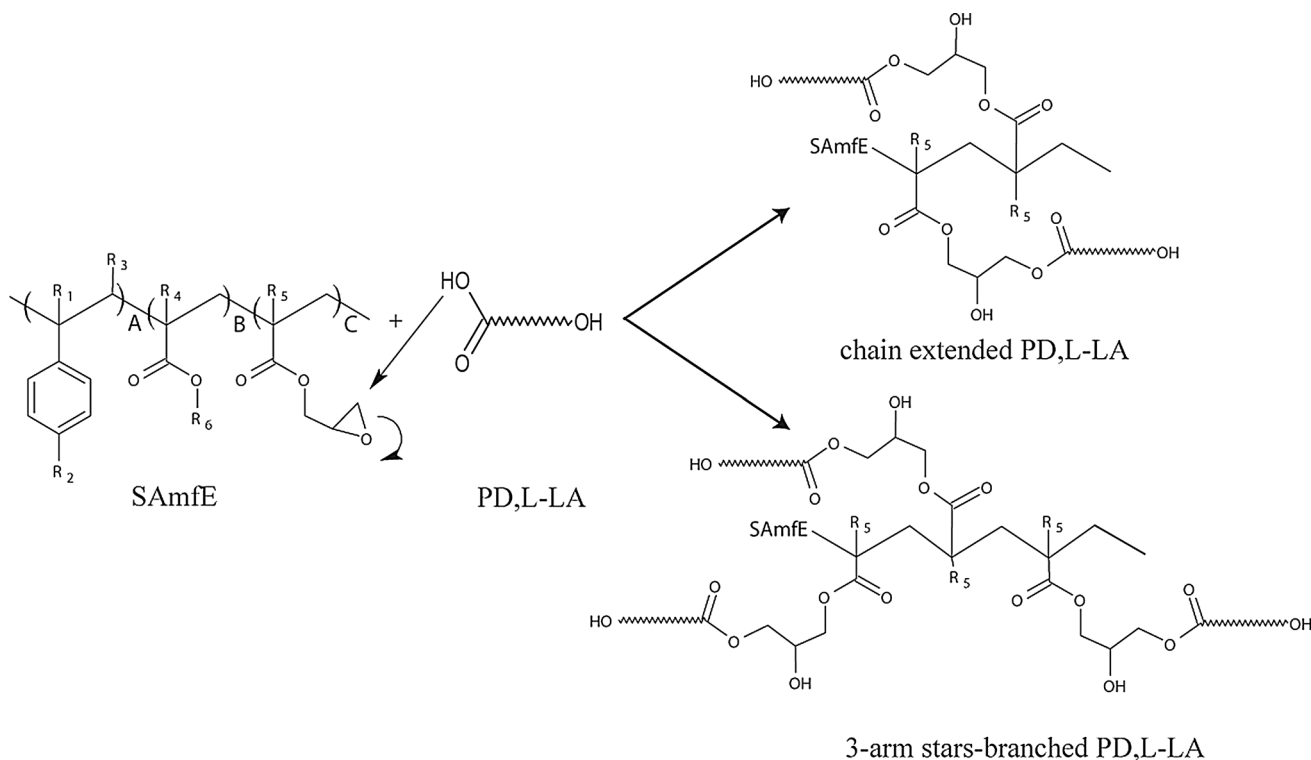


Fig. 1 Topological structures created in REX samples through reactive extrusion process [16]

speed of 1.25 rpm. Figure 1 represents the different topological structures that were generated through reactive extrusion besides the remaining linear one. More details on sample preparation and characterization can be found elsewhere [16].

A thermal treatment was then applied to the sheets in order to release internal stresses and to avoid excessive defects during sample cutting. They were heated to 60 ± 1 °C for 40 min in a convection oven (J.P. Selecta, s.a., Barcelona, Spain) and subsequently quenched in an ice water bath (2 ± 2 °C) for 15 min. After drying, the different samples were immediately extracted from the center of the sheet, parallel to the main axis of the machine direction (MD). On one hand, de-aged samples (referred to as Da) were tested immediately after the end of the thermal treatment. On the other hand, physical aged samples were stored at room temperature for 1 week prior to testing in order to simulate industrial storage conditions. All analyzed samples are specified in Table 1. Samples were distinguished by their topological modifications and their physical aging state.

Thermal characterization

A differential scanning calorimeter (DSC) (Pyris 1 coupled to a 2P intracooler, Perkin Elmer, Waltham, MA, USA) was used. Tests were conducted under dry nitrogen

atmosphere. Temperatures as well as heat of transition were calibrated with lead and indium at 10 °C min^{-1} . 5–6 mg of each sample was encapsulated in aluminum pans. All samples were subjected to a first heating scan from 10 to 200 °C at 10 °C min^{-1} in order to reveal the typical thermal transitions.

To analyze the rate of enthalpy relaxation below T_g , freshly de-aged samples were stabilized at 30 °C; then, predetermined isothermal steps between 0 (only quenched) and 1000 min were performed. Each isothermal step was followed by a rapid quenching to -10 °C at 100 °C min^{-1} where the temperature was equilibrated during 1 min. Samples were then reheated from -10 to 30 °C and from 30 to 80 °C at 50 °C min^{-1} and at 10 °C min^{-1} , respectively. Although the former heating ramp was used to bring samples quickly at room temperature, the latter was programmed to record the DSC trace of the aged state.

As a result of the current aging temperature (30 °C), a significant annealing time is required to reach a complete material structural equilibrium. Therefore, freshly de-aged samples were aged for 6 months at room temperature and thereafter heated from 30 to 80 °C at 10 °C min^{-1} in order to reveal their aged state.

Each of the DSC measurements was repeated three times using fresh samples in order to improve accuracy and to minimize the errors brought by baseline fluctuations and calibrations.

Table 1 Nomenclature used for all analyzed samples in the current study

Extruded material	M_w^a (g mol ⁻¹)	PDI^a	Sample nomenclature	Observations
Linear topology PD,L-LA sheet	179 441	2.1	PLA Da	Samples tested immediately after thermal treatment
			PLA	Samples stored at room temperature for 1 week after thermal treatment and subsequently tested
Long-chain-branching topology PD,L-LA sheet	297 307	2.5	PLA-REX Da	Samples tested immediately after thermal treatment
			PLA-REX	Samples stored at room temperature for 1 week after thermal treatment and subsequently tested

^a The molecular weight average (M_w) and the polydispersity index (PDI) of each sample were determined by size exclusion chromatography (SEC) experiments [16]

From the first heating scan, the degree of crystallinity was determined using Eq. 1.

$$\chi_c(\% \text{Crystallinity}) = 100 \times \frac{\Delta H_m - \Delta H_{cc}}{\Delta H_m^0} \quad (1)$$

where ΔH_m is the melting enthalpy and ΔH_{cc} is the cold-crystallization enthalpy. ΔH_m^0 is the melting enthalpy for a 100 % crystalline PLA sample equal to 93.6 J g⁻¹ [18].

For amorphous polymers, it has been demonstrated that the enthalpy recovered (δ_H) during isothermal enthalpy relaxation experiments depends on several variables [19]. In fact, the cooling rate from the melt, the aging temperature, the aging time as well as the heating rate may affect the configurational rearrangement of the polymer chains over time. As described above, in the present work, all these parameters were kept constant, except for the aging time (t_a). A direct measure of the overall relaxation kinetics of the polymer chains may therefore be provided by these experiments. δ_H was calculated as the difference in area between the DSC trace of isothermal aged samples and the quenched reference sample. The Cowie-Ferguson model was employed to analyze δ_H as a function of t_a (Eq. 2) [13, 20].

$$\delta_H(t_a) = \delta_{H_\infty} \times \left[1 - \exp\left(-\left(\frac{t_a}{\tau_0}\right)^\beta\right) \right] \quad (2)$$

where δ_{H_∞} is the equilibrium enthalpy relaxation for t_a approaching ∞ and τ_0 is the characteristic relaxation time. β ($0 < \beta \leq 1$) is a parameter that characterizes the distribution of relaxation times between molecules. A broad distribution of relaxation times is expected for a small value of β .

According to Nutt et al. [19], the aging kinetics (β_H) of a bulk sample may be estimated from the slope of δ_H as a function of the log (t_a) (Eq. 3).

$$\beta_H = d\delta_H/d(\log t_a) \quad (3)$$

Mechanical and fracture characterization

Tensile tests

The mechanical characterization was carried out using uniaxial tensile tests according to the ASTM D638 standard. Specimens of type I were extracted from the center of the sheet, parallel to the MD direction. The different tests were performed at room temperature (23 ± 3 °C) using a universal testing machine (SUN 2500, GALDABINI, Cardano al Campo, Italy) equipped with a 5-kN load cell at a constant crosshead speed of 10 mm min⁻¹. Deformations were measured with a video extensometer (OS-65D CCD, Minstron, Taipei, Taiwan) coupled to a Windows-based software (Messphysik, Fürstenfeld, Austria). The Young's modulus (E), the yield strength (σ_y), the strain at yield (ϵ_y) and the strain at break (ϵ_b) were determined from the engineering stress–strain curves. Values reported correspond to the average of five valid tests.

Fracture behavior

De-aged samples

As a result of the post-yielding crack propagation features observed in initial tests for these samples, the essential work of fracture (EWF) methodology was used. This concept postulates that when a crack propagates after the generation of an extensive plastic damage zone, the work required for the whole fracture process (W_f) may be partitioned into two additives work terms, considering the zone of the process where it is involved.

$$W_f = W_e + W_p \quad (4)$$

W_e is defined as the essential work of fracture. It is the work necessary for the generation of a new surface, and it usually takes place in the inner fracture process zone. Occurring in the outer process deformation zone (OPDZ)

or plastic zone, W_p is defined as the nonessential work of fracture and it corresponds to the work consumed by several deformation mechanisms (e.g.: crazing, micro-voiding, shear yielding) [4, 21, 22]. Although W_e is considered as a surface-related energy whose value is proportional to the fracture area (lt), W_p is a volume-related energy whose value is proportional to the volume of the deformed zone ($\beta l^2 t$). l and t are defined as the ligament length and the specimen thickness, respectively. β corresponds to the shape factor of the necked zone related to the volume of deformed material surrounding the ligament length, which value depends on the OPDZ geometry. Thus, rearranging Eq. 4, the specific work of fracture (w_f) can be expressed as a function of the ligament length (Eq. 5) [22, 23].

$$W_f/lt = w_f = w_e + \beta w_p l \quad (5)$$

where w_e represents the specific essential work of fracture, and w_p is the specific nonessential work of fracture. Thus, w_e and the plastic term (βw_p) are easily obtained from a linear regression of a set of values represented in a graph plotting w_f versus l . β can be determined from the slope of h versus l linear regression, as defined in Eq. 6.

$$h = k \times \beta \times l \quad (6)$$

h represents the height of the necked zone and according to Ferrer-Balas et al. [24], k is a constant equal to 1.5 due to the parabolic-like form of the necked zone.

Following the recommendations of the European Structural Integrity Society-Technical Committee 4 (ESIS-TC4) [25], the deeply double-edge-notched tension (DDENT) sample geometry was used in order to ensure a low constraint level under fully plastic conditions.

Identical devices as described in the mechanical characterization section were used to perform uniaxial fracture tests and to measure deformation. Tests were performed with a crosshead speed of 1 mm min^{-1} at room temperature ($23 \pm 3 \text{ }^\circ\text{C}$). DDENT samples were mechanized from the center of the sheet, parallel to the MD direction, using the following dimensions: Length $L = 105 \text{ mm}$, width $W = 65 \text{ mm}$, thickness $t = 1 \text{ mm}$ and distance between grips $ZG = 65 \text{ mm}$. Ten ligament lengths ranged between 6 and 24 mm were tested and repeated three times. Before testing, initial cracks were sharpened with a fresh razor blade. After testing, a binocular lens microscope (Carton, Pathumthani, Thailand) was used to determine the accurate ligament lengths (l) and the height (h) of the necked zone surrounding the ligament length. In addition, a video monitoring system (two digital cameras Xenoplan 1.4/23-0.902, Schneider Kreuznach, Bad Kreuznach, Germany) coupled to a optical strain measurement system (ARAMIS[®], GOM GmbH, Braunschweig, Germany) was employed for an advanced strain analysis using digital image correlation (DIC).

Physical aged samples

The brittle behavior of aged samples led to a fast unstable crack propagation under uniaxial loading. As a result of this behavior, the fracture analysis was carried out determining the crack tip opening displacement (CTOD) δ_i at the onset of crack propagation. As pointed out by Anderson [26], in case of pure plane-stress state condition, the energy consumed to initiate the crack propagation (J_0) may be calculated from δ_i and σ_y of its respective material (Eq. 7).

$$J_0 = \sigma_y \times \delta_i \quad (7)$$

In order to avoid problems of crack propagation outside of the ligament plane, single-edge-notched tension (SENT) test geometry was used to perform these tests. They were mechanized from the center of the sheet, parallel to the MD direction, using the following dimensions: Length $L = 140 \text{ mm}$, width $W = 50 \text{ mm}$, thickness $t = 1 \text{ mm}$ and distance between grips $ZG = 100 \text{ mm}$. According to a previous dimensional analysis, these dimensions ensured similar crack tip constraint ahead of the crack tip between DDENT and SENT samples. In order to perform a preliminary inspection of the possible change in the fracture toughness of aged samples, a unique ligament length (l) equal to 20 mm was tested. For each material, five samples were evaluated. The initial crack was sharpened with a fresh razor blade directly after the thermal treatment applied. Prior to testing, a polarized light microscopy (Nikon, Optiphot-Pol XTP-11, Japan) was used to verify the pre-crack quality. No plastic pre-deformation at the crack tip and an extremely sharp crack tip was observed.

Uniaxial tests were performed on a servo-hydraulic testing system (Amsler HC25, Zwick Roell, Ulm, Germany), equipped with a 2-kN load cell, in tensile configuration. Tests were conducted with a crosshead speed of 10 mm min^{-1} at room temperature ($23 \pm 3 \text{ }^\circ\text{C}$). A similar video monitoring system as described above was used for advanced strain analysis using DIC analysis.

Prior to perform DIC analysis, samples were “speckle coated” with white and black aerosol paints in order to create an optically active random structure. During the tests, displacements of this nonuniform surface pattern were recorded by a series of digital images (1600×1200 pixels) at a frame rate of 10 Hz. After testing, the DIC post-test analysis was performed using a commercial DIC software, Aramis[®] (GOM GmbH, Germany). The displacement field ahead of the crack tip was analyzed by viewing a rectangular field of $15.2 \text{ mm} \times 0.46 \text{ mm}$, meshed by square facets (9×9 pixels) with a 3 pixels overlapping area. A full-field three-dimensional measurement of the specimen shape and strain field was thus calculated by deriving these discrete displacements. Using the strain field measurement, δ_i may therefore be determined

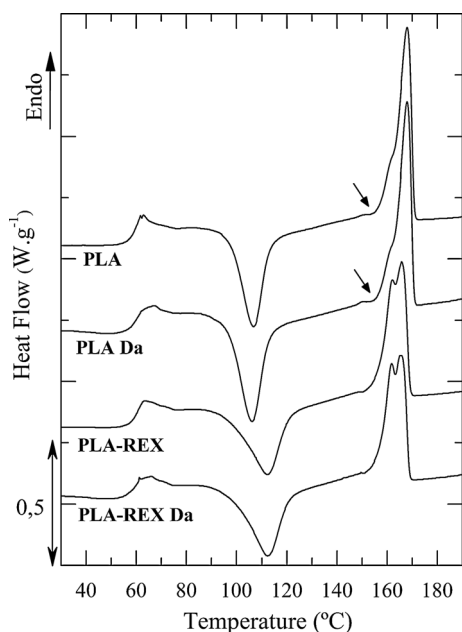


Fig. 2 First DSC heating scan at 10 °C min^{-1} for aged and de-aged samples

just before the crack propagation onset. The CTOD value was measured between two fixed nodes ahead of the initial crack tip.

Fractography characterization

The fractured surfaces of all aged samples (SENT geometry) were inspected by Scanning Electron Microscopy (SEM) (JEOL, JSM-7001F, Tokyo, Japan). Experiments were performed under vacuum with an accelerating voltage of 2 kV. Samples were previously coated with platinum vapor.

Results and discussion

Thermal properties

The first DSC heating scan at 10 °C min^{-1} of all the samples is shown in Fig. 2. Midpoint glass transition

temperature (T_g), cold-crystallization temperature (T_{cc}), cold-crystallization enthalpy (ΔH_{cc}), melting temperature (T_m), melting enthalpy (ΔH_m) and degree of crystallinity (X_c) results are compiled in Table 2.

Under controlled aging periods, structural modifications induced in the PD,L-LA matrix through REX-Calendering process did not affect the midpoint T_g (*c.f.* Table 2). However, as it was expected for aged samples, the endothermic peak intensity related to the enthalpy relaxation observed in the vicinity of T_g was larger compared with the one of de-aged samples. This phenomenon has been extensively studied, and the effects are well established. For aged samples, it was a consequence of a large change in the potential energy in the T_g region due to the alteration of locally ordered domains to a more disordered conformational state, upon heating [3].

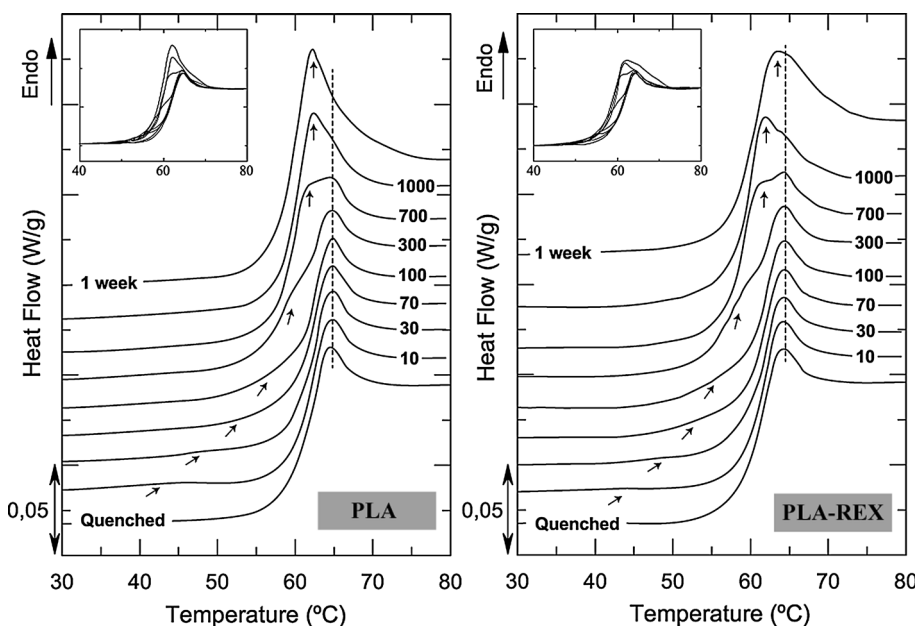
According to X_c values, all samples can be considered to be amorphous due to the low crystalline fraction developed under reactive extrusion (REX) processing conditions. In Fig. 2, it can be observed that the melting transitions of PLA and Poly(lactic acid) de-aged (PLA Da) samples exhibited a small exotherm (indicated by an arrow) prior to the dominant melting transition. According to several studies [27, 28], this exothermic peak may be attributed to the α' -to- α transition of the possible α' -crystals developed during the fast cooling from the melt to an isothermal step at 50 °C (calendering stage). Then, the presence of two overlapped endotherms was proposed to be due to the melt-recrystallization mechanism. The low-temperature shoulder may be attributed to the melting of the original crystals, while the high-temperature endotherm may be attributed to the melting of crystals generated through the melt-recrystallization mechanism upon heating [28].

In contrast, PLA-REX samples exhibited a well-defined double-melting peak which may be attributed to the melting of two different crystalline populations with different lamellar thicknesses and degrees of perfection [29]. The long-chain branching inserted in the PLA matrix may act as structural defects, giving rise to a less crystal perfection (lower lamellar thickness). As it can be observed in Fig. 2, the cold-crystallization peak of all REX samples was shifted to higher temperatures. As a result of the higher content of structural irregularities (long-chain branching)

Table 2 Thermal properties determined from the first DSC heating scan

Sample nomenclature	T_g (°C)	T_{cc} (°C)	ΔH_{cc} (J g ⁻¹)	T_m (°C)	ΔH_m (J g ⁻¹)	X_c (%)
De-aged						
PLA Da	60 ± 1	106 ± 2	31 ± 1	168 ± 1	33 ± 1	2 ± 1
PLA-REX Da	58 ± 1	112 ± 1	28 ± 1	165 ± 2	32 ± 2	4 ± 2
Physical aged						
PLA	59 ± 1	107 ± 1	31 ± 1	168 ± 1	34 ± 1	3 ± 1
PLA-REX	60 ± 1	112 ± 2	28 ± 1	165 ± 2	32 ± 1	4 ± 2

Fig. 3 DSC heating scans at $10\text{ }^\circ\text{C min}^{-1}$ of samples aged at $T_a = T_g - 30\text{ }^\circ\text{C}$ in the glass transition region. Each thermogram was recorded at the indicated aging times (in minutes). Inserts display an overlay of the same curves to justify the correct superimposition of the individual thermograms below and above T_g



coupled with a significant increase in the molecular weight, the polymer chain mobility may be reduced leading to a possible decrease in the ability to crystallize [30].

Structural modification effects on enthalpy relaxation

Figure 3 depicts the different heating scans for PLA and PLA-REX samples aged at $30\text{ }^\circ\text{C}$ ($T_a = T_g - 30\text{ }^\circ\text{C}$) for various aging times (from 0 min to 1 week). In an initial study, due to the repeated isothermal steps, both samples were analyzed for a possible thermal degradation by carefully studying the DSC trace in the glass transition region (from 40 to $80\text{ }^\circ\text{C}$). As it can be seen in the inserts of Fig. 3, all DSC heating scans are well superimposed in the glassy and in the rubbery regions. This indicates that no degradation or irreversible changes did occur and that both samples attain a reproducible state each time they are heated above T_g .

As it can be seen in Fig. 3, although no isothermal aging step was performed on quenched samples, they present an endothermic signal above T_g (overshoot). Therefore, it may be concluded that an enthalpy relaxation process took place in the amorphous phase upon heating to T_g . For isothermally aged samples, besides the constant overshoot above T_g , an additional endothermic signal (indicated by an arrow) was revealed below T_g . The intensity of this additional endotherm increased and shifted to higher temperature with increasing aging time. For samples aged up to 700 min, an overlapped shoulder in the T_g transition appeared which merged with the constant overshoot above T_g when the aging time was further increased. This was due to an increase in the excess enthalpy of relaxation resulting from a substantial decrease in the molecular mobility as the

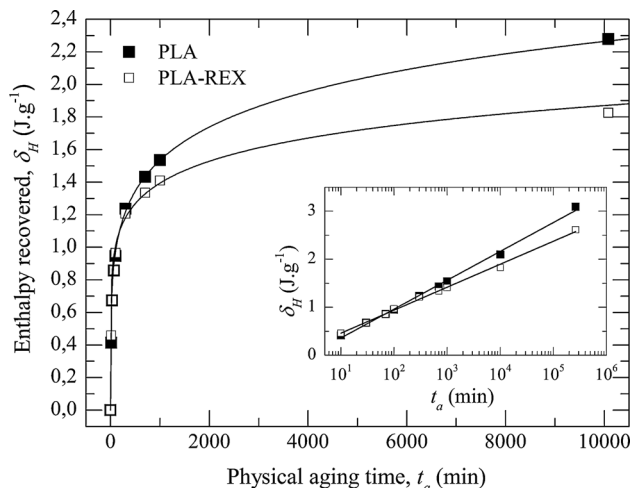


Fig. 4 δ_H as a function of t_a for both samples aged at $T_a = T_g - 30\text{ }^\circ\text{C}$. The Cowie–Ferguson model is fitted for each sample and the insert shows the linear correlation between δ_H and $\log(t_a)$

polymer ages. This observation is in line with the theory proposed by Struik [31] stating that when an amorphous polymer phase is aged at a *sub- T_g* temperature ($T_a - T_g - 20\text{ }^\circ\text{C}$), de-aging process occurs below T_g . The dashed line highlighted the characteristic T_g overshoot displayed by all samples.

Based on the DSC thermograms of Fig. 3, δ_H was determined for each sample and represented as a function of t_a (c.f. Fig. 4). The insert includes also the measurements of samples which were aged for 6 months. The Cowie-Fergusson parameters (c.f. Eq. 2) as well as β_H (c.f. Eq. 3) were calculated for each material and are compiled in Table 3.

Table 3 Cowie–Ferguson model parameters and enthalpy relation kinetics for PLA and PLA-REX samples

Sample nomenclature	PLA	PLA-REX
$\delta_{H\infty}(\text{J g}^{-1})^a$	3.1 ± 0.2	2.6 ± 0.2
$\tau_0 (10^3) (\text{min})$	18 ± 3	110 ± 20
β	0.26 ± 0.01	0.17 ± 0.01
$R^2 (\delta_H \text{ vs. } t_a)$	0.993	0.981
$\beta_H (\text{J g}^{-1} \text{ per decade})$	0.56 ± 0.01	0.47 ± 0.01
$R^2 (\delta_H \text{ vs. } \log(t_a))$	0.999	0.995

^a $\delta_{H\infty}$ was determined by DSC tests of samples aged for 6 months at room temperature

The numerical values of the experimental fits may be considered as reliable due to the high correlation coefficient ($R^2 (\delta_H \text{ vs. } t_a)$) obtained for both samples (*c.f.* Table 3). In addition, a linear relationship was established for the enthalpy recovered as a function of $\log(t_a)$. This observation indicates a proper fitting of the experimental data and is in good agreement with previous published data [5, 13, 32].

As it can be seen in Fig. 4, δ_H increased rapidly for both samples when the aging time was increased to 700–1000 min. However, as the aging time further increased, the enthalpy-recovered content was lowered for PLA-REX samples as compared to PLA samples. During physical aging process, Pan et al. [5] suggested that the decrease in the free volume (v_f) in amorphous PLLA involves a change in the molecular chain conformation from totally disordered for unaged materials to locally ordered for aged ones. As mentioned earlier, it has been established that relaxations in the amorphous phase were mainly controlled by the entangled network density. Since REX samples presented a higher number of physical crosslinking points, disentanglement and unknotting process rates of the chains in the experimental timeframe may be slowed down, decreasing thereby the rate of enthalpy relaxation, β_H . As shown in Table 3, this β_H slowdown broadened the distribution of relaxation time (lower β) and increased τ_0 .

Tensile properties

The typical tensile engineering stress–strain curves of all samples are shown in Fig. 5. It can be appreciated that de-aged PLA samples behaved in a ductile manner while aged samples featured a brittle behavior. Considering aged samples, it should be noted that both materials presented a local maximum in the engineering stress which may be associated with a yield point. However, the formation of crazes prevented the propagation of a stable neck, giving rise to a premature brittle fracture. Table 4 summarizes the mechanical parameters of all samples.

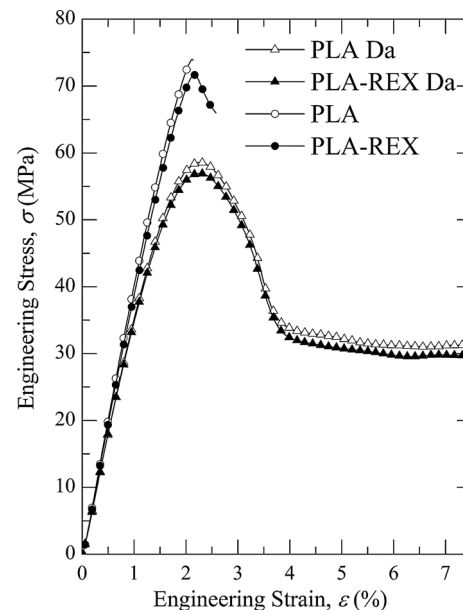


Fig. 5 Typical tensile engineering stress–strain curves at 10 mm min^{-1}

After testing, a visual inspection of both aged samples (*c.f.* Fig. 6) revealed that PLA samples exhibited several long plane crazes surrounding only the fractured zone. This scenario changed substantially when PLA-REX samples were considered. A larger stress-whitened zone was observed in the calibrated zone. A more detailed inspection of the fractured region revealed a larger proportion of shorter crazes, which became thinner and better defined. The irregularities present in the molecular pattern coupled with a higher entangling knots density might have stopped the growth of long crazing planes and promoted the formation of various shorter ones under loading [33, 34]. This larger content of highly localized process plastic yielding that surrounds crazes led to a slight increase in ϵ_b for REX samples (*c.f.* Table 4). However, according to Table 4 and taking into account the standard deviations, E , σ_y and ϵ_y did not seem to be affected by the increase in the entanglement network density.

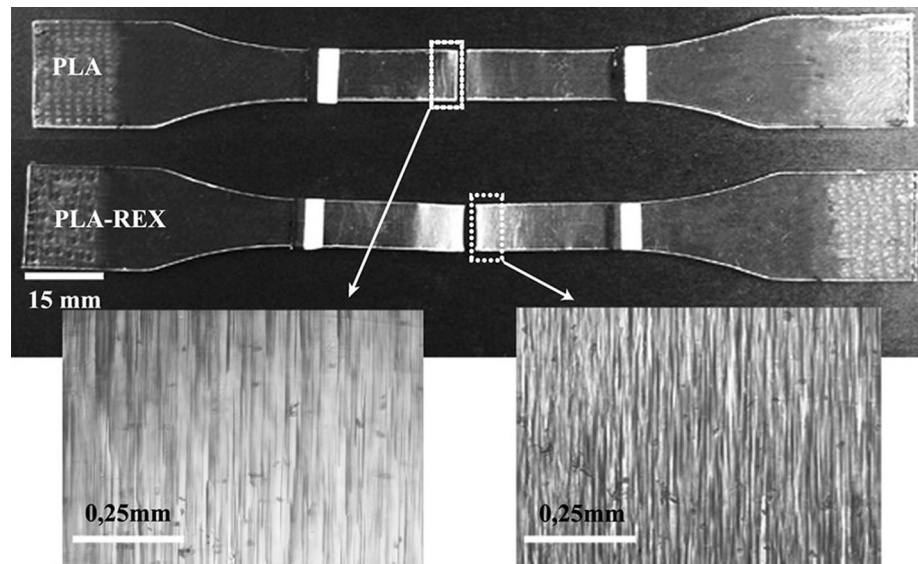
As mentioned previously, de-aged samples showed the typical behavior of ductile polymers with stable neck propagation up to $<100\%$ of their initial length owing to the cold drawing process (*c.f.* Fig. 5 and Table 4). As a result of the larger amount of free volume (v_f) induced by the de-aging thermal treatment, the chain mobility was increased giving rise to a more pronounced anelastic region and a decrease in σ_y [4, 35]. The rupture of locally ordered domains and the larger v_f led to a polymer chain conformation more irregular and more free. These higher-disordered chain arrangements may have therefore induced a larger proportion of twisted chains possibly leading to a similar average dynamic environment of the entangled

Table 4 Uniaxial tensile parameters at 10 mm min^{-1}

Sample nomenclature	E (GPa)	σ_y (MPa)	ε_y (%)	ε_b (%)	X_c (%) ^a
De-aged					
PLA Da	3.2 ± 0.2	58.7 ± 0.5	2.29 ± 0.02	165 ± 10	16 ± 2
PLA-REX Da	3.3 ± 0.1	57.6 ± 0.8	2.26 ± 0.04	165 ± 5	12 ± 1
Physical aged					
PLA	3.5 ± 0.1	74 ± 2	2.2 ± 0.1	2.2 ± 0.1	–
PLA-REX	3.3 ± 0.1	73 ± 1	2.18 ± 0.03	2.5 ± 0.1	–

^a The tested specimens were cut from the necked zone of tensile samples stretched at 100 % of their initial length. X_c values were determined from the first DSC heating scan at $10 \text{ }^\circ\text{C min}^{-1}$ and repeated three times for each material

Fig. 6 Light macrophotographs of aged PLA and PLA-REX specimens after testing at 10 mm min^{-1} . Micrographs were taken from the surrounding fractured part of each sample



polymer coils between both de-aged materials. Similar polymer coils and segment mobility may have been present, leading to analogous mechanical properties for both materials.

Nevertheless, a slight visual difference may be appreciated if the stretched region of both samples was considered. As shown in Fig. 7, the whitening of the stretched region was less pronounced for PLA-REX samples as compared to PLA samples. Similar to PET polymer, this whitening is usually attributed to the strain-induced crystallization effect. However, according to several authors [36, 37], stretching of the PLA polymer does not induce a stable crystal formation. A mesomorphic phase is generated whose conformation and dimensional parameters are close to those of stable crystals but without regular spacing. Then, further heating will bring enough energy to this metastable crystal form to transform into a stable crystal one with a lowered energetical conformation. According to the degree of crystallinity (*c.f.* Table 4) obtained after heating the stretched samples up to $200 \text{ }^\circ\text{C}$, the ability to generate a crystalline state seemed to be reduced when PLA-REX samples were stretched. This decrease in the

ability to “crystallize” upon stretching may be due to the increase in the sample molecular weight coupled with the introduction of long-chain branching.

Fracture behavior

Essential work of fracture

According to the ESIS-TC4 protocol [25], three main preconditions have to be fulfilled in order to analyze properly the EWF results: (1) the ligament length (l) of the DDENT specimens must be in a range that guarantees a full ligament yielding before the crack propagation onset; (2) a self-similarity of the load-deformation curves for each ligament length in order to assure a similar fracture process between all of them and (3) the process must take place in a pure plane-stress state condition for the whole range of l under study [4, 23].

For both de-aged materials, the self-similarity criterion of the load-deformation curves was verified during tests, in the range of l under study. Figure 8 displays the engineering stress as a function of the normalized displacement

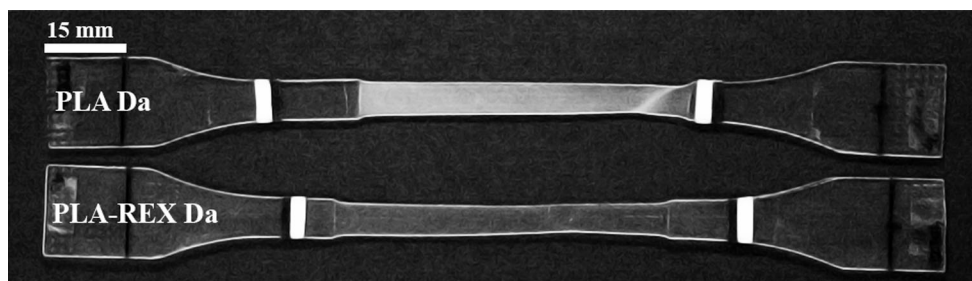
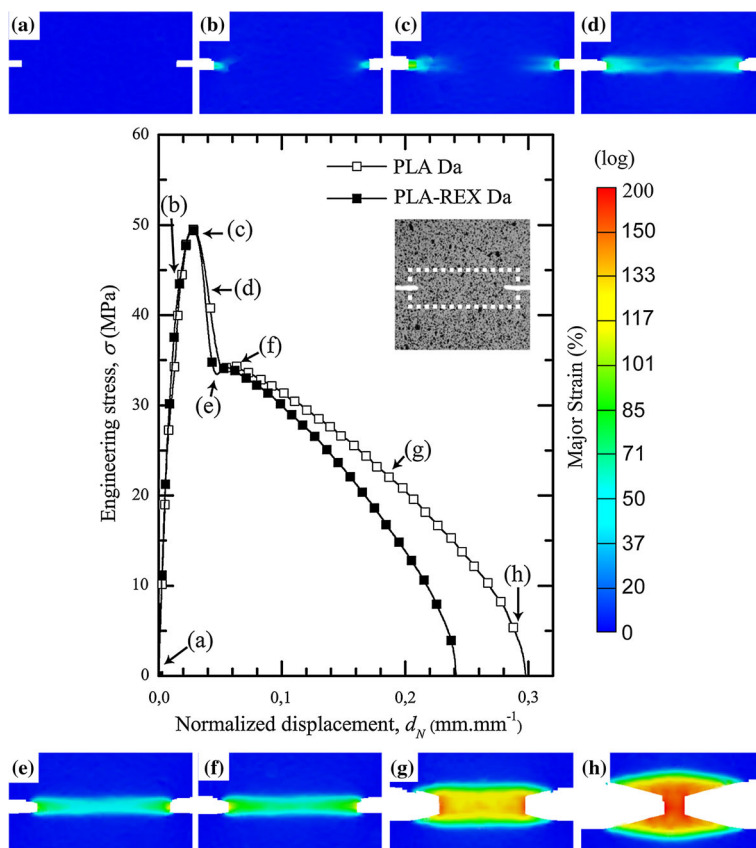


Fig. 7 Visual aspect of the necked region of de-aged PLA and PLA-REX samples stretched at 100 % of their initial length

Fig. 8 Engineering stress versus normalized displacement (by an l of 18 mm) curves for DDENT samples tested at 1 mm min^{-1} . The strain field surrounding the ligament length was determined in some characteristic points by DIC analysis in the rectangular field (white dashed line, insert)



curves for de-aged PLA and PLA-REX samples. The strain field determined by DIC analysis suggested that the onset of yield appeared in point b. Yielding process was initiated well before the maximum stress and from both sharpened cracks due to the high stress concentration ahead of notches. At point e, the ligament was fully yielded and the crack propagation was initiated, which fulfilled the pre-condition of total plastic collapse of the ligament prior to crack initiation. As it can be seen in Fig. 9, the linear relationship between the specific work of fracture (w_f) and l confirmed that the fracture process took place in uniform stress state (pure plane stress in this case) and that Eq. 5 can be used for the analysis. Characteristic EWF parameters' results are compiled in Table 5.

According to Table 5 and taking into account the experimental error involved, structural modifications induced by reactive extrusion did not seem to affect the work required for the onset of crack propagation; associated with the essential term (w_e). Similar w_e values were determined by Gámez-Pérez et al. [4] for de-aged PLA films with a nominal thickness of 0.3 mm. Under plane-stress condition, this present observation is in line with previous communications stating that for amorphous polymers, w_e is a material constant, independent of the specimen geometry and molecular weight [38, 39].

Although βw_p remained constant between both materials when the experimental error was taking into account, a different post-yielding behavior may be appreciated by

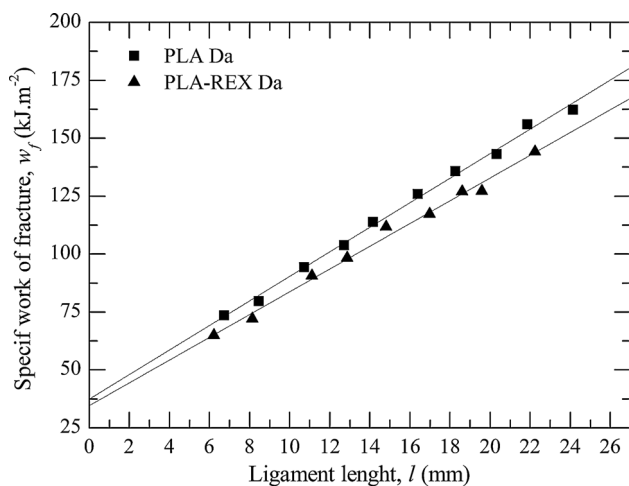


Fig. 9 w_f as a function of l for DDENT samples

considering Fig. 8. Therefore, a detailed analysis of this term was necessary to elucidate the effects of the increase in v_e due to the long-chain-branching topology generated through REX processing on the nonessential term. As it can be seen in Table 5, the shape factor β was lowered when v_e was increased, indicating a significant decrease in the volume of deformed material surrounding the ligament length. A significant rise in w_p was thereafter obtained, indicating an increase in the energy density dissipated in the deformation process surrounding the plane of crack propagation.

In order to give a physical meaning to the trends obtained by the above parameters, the deformation process has to be considered. According to Karger-Kocsis et al. [40], shear banding via network stretching appeared to be the dominant deformation mechanism in the whole process zone (IPFZ and OPDZ) of amorphous thermoplastic polyesters. For ductile amorphous polymers, this deformation process (network stretching) agrees thereby with the physical interpretation of the EWF parameters presented by Chen et al. [37]. Under loading, the network stretches until a “locked” point, governed by the entangled knots which act as chemical crosslinking points. Once this “locked” point is reached, the covalent bonds of the entangled chains ahead of the crack tip are stretched to a critical value and finally break, leading to crack propagation. Thus, the content and the degree of viscoelastic and viscoplastic flow that may undergo the molecular network prior to reach the “locked” point governs the size and energy density surrounding the crack propagation plane.

Regarding the materials of the present study, this network stretching mechanism was confirmed when a complete recovery of the stretched region of the tested samples was observed after being placed above T_g for 10 min. At the testing temperature, both samples presented a significant molecular relaxation time, suggesting that entangling knots may have acted as “chemical” crosslinking points [16]. Thus, under uniaxial loading, as long as disentanglements did not take place, the deformation mechanism governing the network stretching was principally dependent of the entangled network. Beyond the yield point, a more entangled network may accommodate lower network extension as compared to a less-entangled structure. This was attributed to the fact that the molecular weight between entanglements was reduced giving rise to a lowered backbone stretching level. Therefore, they were able to distribute and relieve the stress in a smaller volume element (lower β value). In addition, in a highly entangled network, the mechanical work content necessary to generate the plastic flow was supposed to increase, leading to a higher w_p value. This was due to a decrease in the ability to orientate the molecular chains under uniaxial loading [41, 42].

Despite these last differences, the global parameters (w_e and βw_p) did not seem to be influenced by the structural modifications induced through one-step reactive calendaring process for de-aged materials.

Fracture toughness of aged samples

As previously mentioned, an inspection of the possible changes in fracture toughness of all aged samples was assessed by the determination of the CTOD (δ_i). According to DIC analysis, Fig. 10 shows the resulting strain field ahead of the crack tip, at the onset of the crack propagation. Numerical parameters are compiled in Table 6. As it can be seen in Fig. 10, PLA samples exhibited a larger blunting ahead of the crack tip as compared to PLA-REX ones, leading to a wider δ_i before the catastrophic crack propagation (*c.f.* Table 6). As a result of this larger strain and considering that both samples have a similar σ_y (*c.f.* Table 4), PLA samples presented a higher energy consumption up to the crack propagation onset as compared to PLA-REX samples.

In order to obtain more information about the fracture process, SEM analysis was performed on the fractured surfaces of both aged samples. Figure 11 shows an

Table 5 Influence of the structural modifications on the EWF parameters

Sample nomenclature	w_e (kJ m ⁻²)	βw_p (MJ m ⁻³)	β (10 ⁻²)	w_p (MJ m ⁻³)	R^2 (w_f vs. l)
PLA Da	37 ± 2	5.3 ± 0.1	8.3 ± 0.6	63.9 ± 0.1	0.998
PLA-REX Da	34 ± 2	4.9 ± 0.2	6.1 ± 0.5	80.3 ± 0.2	0.996

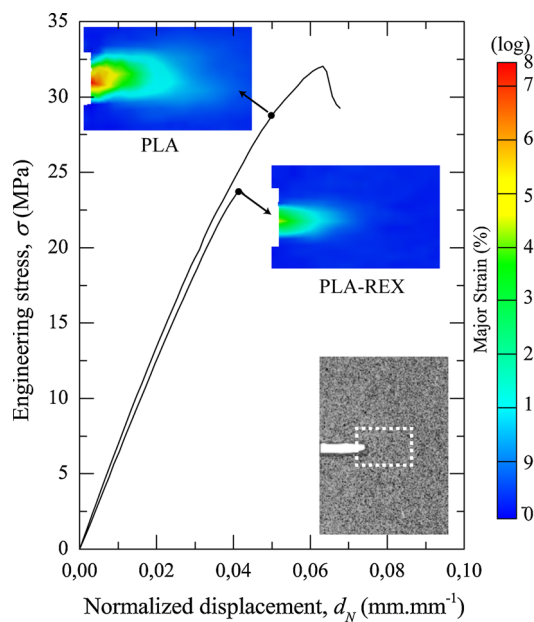


Fig. 10 Engineering stress versus normalized displacement (by l of 20 mm) for aged PLA and PLA-REX samples. The strain field ahead of the crack tip was determined by DIC analysis in the rectangular field (white dashed line, insert)

Table 6 Influence of the entanglement network density on the CTOD and J_0 parameters

Sample nomenclature	δ_i (mm)	J_0 (kJ m ⁻²)
PLA	0.31 ± 0.02	23 ± 2
PLA-REX	0.18 ± 0.05	13 ± 1

overview of the fractured ligament length together with two detailed regions for aged PLA and PLA-REX samples.

As it can be seen in Fig. 11, both samples exhibited two different regions with different fracture surface features. Ahead of the crack tip, the first zone (referred to as surface 1) showed a smooth topography with only few cuts running perpendicular to the propagation direction. As a result of the smooth feature of this surface coupled with the absence of plastic tearing, this region may characterize the controlled propagation step of the crack propagation. Thus, the crack propagation onset was preceded by a long craze growth whose growth rate ($V_{\text{craze-growth}}$) was faster than the crack propagation rate (V_{crack}).

The second zone (referred to as surface 2) showed evidences of random nucleation, orientation and size of crazes in which thin fibrils may be observed. This surface topography is usually called “hackled” pattern and is

characteristic of a brittle behavior. Regarding polymeric materials, this situation is expected when V_{crack} exceeds $V_{\text{craze-growth}}$. In this region, craze nucleation and craze growth processes were uncontrolled and erratic under uniaxial loading which means that the unstable regime of crack propagation was reached.

Although surface 1 recovered two-thirds of the PLA ligament length samples with a slight reduction of its initial thickness (delimited by the black dashed line), this length was reduced to less than half of the fractured ligament length for PLA-REX samples with no evidences of substantial thickness reduction. These observations indicated that PLA-REX samples achieved less craze thickening prior to the craze–crack transition as compared to PLA samples. This may be due to the lower molecular mobility under loading as a result of the higher entangling knots density. Therefore, the mechanical work underwent by the matrix at the onset of crack propagation was lowered, giving rise to lowered J_0 values. Regarding PLA samples, this “delayed” craze–crack transition was highlighted in Fig. 10 by the further increase in the engineering stress up to a local maximum after the onset of crack propagation.

As shown in Fig. 11 for PLA-REX samples, surface 2 presented a larger surface together with a higher number of craze random nucleation. This observation is in line with the behavior previously observed in tensile tests where a larger content of short and thin crazes was generated when PLA-REX samples were loaded in mode I. Although no significant differences were observed in the tensile test parameters between both aged materials (*c.f.* Table 4), in this section the CTOD analysis revealed a significant difference between both of them. Therefore, in the presence of a stress intensifier (notch), an increase in the entangling knot density may lead to a loss of stability in the crack propagation process.

Under pure plane-stress state condition, Wu et al. [43] stated that w_e obtained by the EWF methodology is equivalent to J_0 . A possible comparison between the EWF parameters determined in the above section and the J_0 parameter was therefore possible in the current study due to the fact that both (w_e and J_0) are independent of the geometry employed [39, 43, 44]. As a result of a decreased ability to dissipate energy through molecular motion, aged samples showed a decrease in the energy consumed by the material in order to initiate the crack propagation (*c.f.* Table 5 and 6). Therefore, in this latter state, as a result of a less stretchable chain network due to a higher entangling knots density, changes in the fracture toughness were more pronounced.

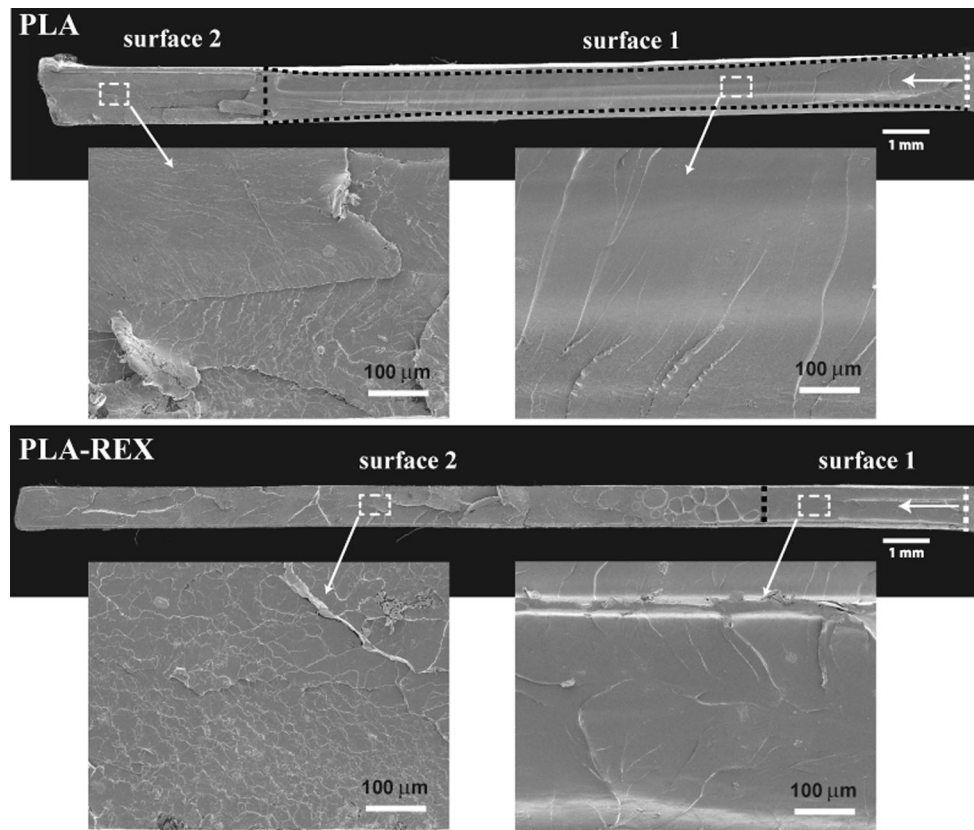


Fig. 11 SEM micrographs of the total fractured ligament length and of two characteristic fractured surfaces for PLA and PLA-REX samples. The white arrow indicates the crack propagation direction ahead of the crack tip

Conclusions

Under the REX-calendering processing conditions employed in the current study, DSC results suggested a decrease in the crystallization ability for REX samples as a result of a slight increase in the cold-crystallization temperature. In addition, the molecular weight increase coupled with the generation of long-chain branching may have changed the melting mechanisms from the melt-recrystallization to the multiple lamellae population mechanism for REX samples. Under controlled aging periods at 30 °C, the rate of enthalpy relaxation presented by the modified samples was slowed down. A higher entanglement network density is therefore a good way to reduce the ability of reorganization toward a more ordered conformational state of the amorphous PD,L-LA biopolymer over time.

Aged REX samples subjected to uniaxial loading presented a slight increase in the strain at break as a result of a larger nucleation of highly localized process plastic yielding zones in various different planes. This phenomenon was promoted by the higher content of irregularities present in their respective molecular pattern. In contrast, as a result of a larger free volume, the average dynamic environment of the entangled polymer coils in both

samples was likely similar, leading to similar mechanical properties for both de-aged samples.

Topological changes in the de-aged samples did not affect the specific work of fracture associated with the work required for the onset of crack propagation (w_c). However, the higher entanglement network density presented by REX samples led to a less stretchable network, which might have reduced the viscoplastic flow ahead of the crack tip, promoting a decrease in the volume of deformed material surrounding the ligament length. Although the same molecular restriction effects led to an increase in the strain energy necessary to reach this plastic collapse, the specific nonessential work of fracture (βw_p) associated with the resistance to crack propagation remained constant between both samples.

The analysis of the fracture behavior of aged samples revealed that the crack propagation process was the result of the craze–crack transition phenomenon. As compared to PLA-REX samples, this transition was delayed for PLA samples allowing thereby a larger CTOD prior to the onset of crack propagation which led to higher J_0 values. Regarding PLA-REX samples, the presence of a denser entanglement network restricted the network extensibility limiting thereby the craze thickening. Therefore, the craze–

crack transition took place earlier giving rise to a higher crack propagation instability.

Acknowledgments The authors would like to thank the MICINN (Spain), the projects financial support MAT2010-19721-C02-01, MAT2010-19721-C02-02 and BASF® for kindly supplying the reactive agent.

References

- Miyata T, Masuko T (1998) Crystallization behaviour of poly(L-lactide). *Polymer* 39:5515–5521
- Nyambo C, Misra M, Mohanty AK (2012) Toughening of brittle poly(lactide) with hyperbranched poly(ester-amide) and isocyanate-terminated prepolymer of polybutadiene. *J Mater Sci* 47:5158–5168
- Pan P, Zhu B, Dong T et al (2008) Conformational and microstructural characteristics of poly(L-lactide) during glass transition and physical aging. *J Chem Phys* 129:184902
- Gamez-Perez J, Velazquez-Infante JC, Franco-Urquiza E et al (2011) Fracture behavior of quenched poly(lactic acid). *Express Polym Lett* 5:82–91
- Inoue Y, Pan PJ, Zhu B (2007) Enthalpy relaxation and embrittlement of poly(L-lactide) during physical aging. *Macromolecules* 40:9664–9671
- Lim LT, Cink K, Vanyo T (2010) Processing of poly(lactic acid). In: Auras R, Lim LT, Selke SEM HT (eds) *Poly(lactic acid): synthesis, structures, properties, processing and applications*. Wiley, Hoboken, USA, pp 191–216
- Lim LT, Auras R, Rubino M (2008) Processing technologies for poly(lactic acid). *Prog Polym Sci* 33:820–852
- Joziasse CAP, Veenstra H, Grijpma DW, Pennings AJ (1996) On the chain stiffness of poly(lactide)s. *Macromol Chem Phys* 197:2219–2229
- Fetters LJ, Lohse DJ, Richter D, Witten TA, Zirkel A (1994) Connection between polymer molecular-weight density, chain dimensions, and melt viscoelastic properties. *Macromolecules* 27:4639–4647
- Grijpma DW, Penning JP, Pennings AJ (1994) Chain entanglement, mechanical-properties and drawability of poly(lactide). *Colloid Polym Sci* 272:1068–1081
- Egan BJ, Delatycki O (1995) The morphology, chain structure and fracture-behavior of high-density polyethylene. 2 Static fatigue fracture testing. *J Mater Sci* 30:3351–3357
- Na B, Lv RH, Zhang Q, Fu Q (2007) Macroscopic deformation and failure of ductile polyethylene: the dominant role of entangled amorphous network. *Polym J* 39:834–840
- Tangpasuthadol V, Shefer A, Hooper KA, Kohn J (1996) Thermal properties and physical ageing behaviour of tyrosine-derived polycarbonates. *Biomaterials* 17:463–468
- Raquez JM, Narayan R, Dubois P (2008) Recent advances in reactive extrusion processing of biodegradable polymer-based compositions. *Macromol Mater Eng* 293:447–470
- Carlson D, Dubois P, Nie L, Narayan R (1998) Free radical branching of polylactide by reactive extrusion. *Polym Eng Sci* 38:311–321
- Cailloux J, Santana OO, Franco-Urquiza E et al (2013) Sheets of branched poly(lactic acid) obtained by one step reactive extrusion calendaring process: melt rheology analysis. *Express Polym Lett* 7:304–318
- Nature Works (2005) PLA Polymer 4032D. <http://www.natureworkslc.com/Technical-Resources/4-Series>. Accessed 14 February 2011
- Perego G, Cella GD (2010) Mechanical Properties. In: Auras R, Lim LT, Selke SEM HT (eds) *Poly(lactic acid): synthesis, structures, properties, processing and applications*. Wiley, Hoboken USA, pp 141–153
- Lu HB, Nutt S (2003) Restricted relaxation in polymer nanocomposites near the glass transition. *Macromolecules* 36:4010–4016
- Hay JN (1995) The physical aging of amorphous and crystalline polymers. *Pure Appl Chem* 67:1855–1858
- Lach R, Schneider K, Weidisch R, Janke A, Knoll K (2005) Application of the essential work of fracture concept to nanostructured polymer materials. *Eur Polym J* 41:383–392
- Mazidi MM, Aghjeh MKR, Abbasi F (2012) Evaluation of fracture toughness of ABS polymers via the essential work of fracture (EWF) method. *J Mater Sci* 47:6375–6386
- Maspoch ML, Henault V, Ferrer-Balas D, Velasco JI, Santana OO (2000) Essential work of fracture on PET films: influence of the thickness and the orientation. *Polym Test* 19:559–568
- Ferrer-Balas D, Maspoch ML, Martinez AB, Santana OO (2001) Influence of annealing on the microstructural, tensile and fracture properties of polypropylene films. *Polymer* 42:1697–1705
- Clutton EQ (2001) Essential Work of Fracture. In: Moore DR, Pavan A, Williams JG (eds) *Fracture mechanics testing methods for polymers, adhesive and composites*. Elsevier, Oxford, pp 177–202
- Anderson TL (1995) *Fracture mechanics: fundamentals and applications*, 2nd edn. CRC Press, Boca Raton (USA)
- Inoue Y, Pan P, Kai W, Zhu B, Dong T (2007) Polymorphous crystallization and multiple melting behavior of Poly(L-lactide): molecular weight dependence. *Macromolecules* 40:6898–6905
- Pan PJ, Zhu B, Kai WH, Dong T, Inoue Y (2008) Polymorphic transition in disordered poly(L-lactide) crystals induced by annealing at elevated temperatures. *Macromolecules* 41:4296–4304
- Gong SQ, Pilla S, Kramschuster A, Yang LQ, Lee J, Turng LS (2009) Microcellular injection-molding of polylactide with chain-extender. *Mat Sci Eng C-Bio S* 29:1258–1265
- Kim SH, Kim YH (1999) Direct condensation polymerization of lactic acid. *Macromol Symp* 144:277–287
- Struik LCE (1986) Physical Aging: Influence on the Deformation Behavior of Amorphous Polymers. In: Brostow W, Corneliusen RD (eds) *Failure of plastics*. Hanser, Munich, pp 209–234
- Hutchinson JM, Smith S, Horne B, Gourlay GM (1999) Physical aging of polycarbonate: enthalpy relaxation, creep response, and yielding behavior. *Macromolecules* 32:5046–5061
- Hsiao CC, Sauer JA (1950) On crazing of linear high polymers. *J Appl Phys* 21:1071–1083
- Deblieck RAC, van Beek DJM, Remerie K, Ward IM (2011) Failure mechanisms in polyolefines: the role of crazing, shear yielding and the entanglement network. *Polymer* 52:2979–2990
- Yoshioka T, Kawazoe N, Tateishi T, Chen GP (2011) Effects of structural change induced by physical aging on the biodegradation behavior of PLGA films at physiological temperature. *Macromol Mater Eng* 296:1028–1034
- Stoclet G, Seguela R, Lefebvre JM, Rochas C (2010) New insights on the strain-induced mesophase of poly(D, L-lactide) in situ WAXS and DSC study of the thermo-mechanical stability. *Macromolecules* 43:7228–7237
- Velazquez-Infante JC, Gamez-Perez J, Franco-Urquiza EA, Santana OO, Carrasco F, Maspoch ML (2013) Effect of the unidirectional drawing on the thermal and mechanical properties of PLA films with different L-isomer content. *J Appl Polym Sci* 127:2661–2669
- KargerKocsis J, Moskala EJ (1997) Relationships between molecular and plane-stress essential work of fracture parameters in amorphous copolyesters. *Polym Bull* 39:503–510
- Martinez AB, Gamez-Perez J, Sanchez-Soto M, Velasco JI, Santana OO, Maspoch ML (2009) The essential work of fracture

- (EWF) method—analyzing the post-yielding fracture mechanics of polymers. *Eng Fail Anal* 16:2604–2617
40. Karger-Kocsis J, Czigany T (2000) Strain rate dependence of the work of fracture response of an amorphous poly(ethylene-naphthalate) (PEN) film. *Polym Eng Sci* 40:1809–1815
 41. Chen HB, Wu JS (2007) Understanding the underlying physics of the essential work of fracture on the molecular level. *Macromolecules* 40:4322–4326
 42. Basu S, Mahajan DK, Van der Giessen E (2005) Micromechanics of the growth of a craze fibril in glassy polymers. *Polymer* 46:7504–7518
 43. Wu JS, Mai YW (1996) The essential fracture work concept for toughness measurement of ductile polymers. *Polym Eng Sci* 36:2275–2288
 44. Hashemi S (1997) Work of fracture of PBT/PC blend: effect of specimen size, geometry, and rate of testing. *Polym Eng Sci* 37:912–921